

# Nanosurface Energy Transfer Based Highly Selective and Ultrasensitive “Turn on” Fluorescence Mercury Sensor

Probir Kumar Sarkar,<sup>†</sup> Nabarun Polley,<sup>†</sup> Subhananda Chakrabarti,<sup>‡</sup> Peter Lemmens,<sup>§,||</sup> and Samir Kumar Pal<sup>\*,†</sup>

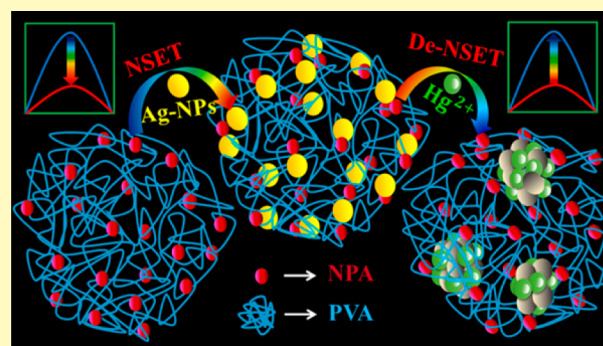
<sup>†</sup>Department of Chemical, Biological and Macromolecular Sciences, S. N. Bose National Centre for Basic Sciences, Block JD, Sector III, Salt Lake, Kolkata 700106, India

<sup>‡</sup>Department of Electrical Engineering, Indian Institute of Technology Bombay, Powai, Mumbai 400 076, Maharashtra, India

<sup>§</sup>Institute for Condensed Matter Physics, and <sup>||</sup>Laboratory for Emerging Nanometrology, TU Braunschweig, Mendelssohnstrasse 3, 38106 Braunschweig, Germany

**ABSTRACT:** Mercury is highly toxic to human health in all of its oxidation states. Thus, developing a low cost, efficient metal ion sensor for the detection of mercury ions at concentration levels down to parts-per-billion (ppb) remains a challenge. In the present work, we have developed a silver nanoparticles (Ag-NPs) impregnated poly(vinyl alcohol) capped 4-nitrophenylanthranilate (PVA-NPA) complex for mercury detection. The fluorescence intensity of the synthesized PVA-NPA is found to be quenched by the impregnated Ag-NPs through dynamic quenching. Moreover, energy transfer (ET) between the acceptor (Ag-NPs) and the donor (PVA-NPA) is observed to follow the nanosurface energy transfer (NSET) mechanism. We have utilized the amalgamation of Ag-NPs with Hg<sup>2+</sup> to develop a low cost prototype, which is highly efficient NSET based ultrasensitive “turn on” fluorescence mercury sensor. This sensor has high selectivity for Hg<sup>2+</sup> ions over a wide range of other competing heavy metal ions, generally present in water of natural sources. The sensor response is found to be linear over the Hg<sup>2+</sup> ions concentration regime from 0 to 1 ppb with a lower detection limit of 100 ppt (0.5 nM). The proposed method demonstrated successfully for monitoring trace Hg<sup>2+</sup> ions in real world samples.

**KEYWORDS:** fluorescence quenching, silver nanoparticles, energy transfer, mercury ions, “turn on” fluorescence, NSET sensor



Mercury is an environmental pollutant and detrimental to human health due to its high toxicity in all oxidation states. Furthermore, mercury is heavily spread out in water, air, soil, and our daily food.<sup>1–5</sup> Such mercury exposure has serious detrimental effects on the brain, heart, lungs, kidneys, central nervous system, and immune system in humans and animals at all ages.<sup>4,6–8</sup> One of the most usual and stable forms of mercury pollution is water-soluble oxidized divalent mercury (Hg<sup>2+</sup>) ions,<sup>7,9</sup> with the maximum permissible level in drinking water and food being ~2 ppb.<sup>10,11</sup> Therefore, the environmental monitoring and determination of low level (sub ppb) concentrations of aqueous Hg<sup>2+</sup> heavy metal ions has become a vital as well as essential need for our healthy society. Several sensitive and selective methods have been developed for qualitative or quantitative detection of Hg<sup>2+</sup> ion using various analytical sophisticated instruments. Most of the instrumental detection mechanism displayed limitations in practical use, such as the time-consuming detection process and in certain cases the applications are unstable or not functional in aqueous media.<sup>12,13</sup> To resolve such issues, noble metal nanoparticles (NPs) are extensively used in the past few years for high sensitive, selective and cost-effective fluorescence based sensor development. Recently, with the development of nano-

technology, fluorescence quenching of fluorescent dyes by noble metal NPs have attracted remarkable attention in biophotonics, material sciences, as well as sensor applications.<sup>14,15</sup> Noble metal NPs, in particular, silver nanoparticles (Ag-NPs), have recently emerged as an important quencher in energy transfer/quenching based fluorescence sensor because of their, strong absorption of electromagnetic waves in the visible region due to Surface Plasmon Resonance (SPR) bands and tunable optical properties induced by small changes in size, shape, surface nature and dielectric properties of the media.<sup>7,16,17</sup> Ag-NPs based sensors are relatively most efficient and sensitive compared to Au-NPs based sensors because of the (more than 100-fold) higher visible region molar extinction coefficient of the Ag-NPs ( $1 \times 10^8$ – $6 \times 10^{10} \text{ M}^{-1} \text{ cm}^{-1}$ ) compared to Au-NPs.<sup>18,19</sup> Although, Au-NPs have been widely employed as colorimetric reporters due to the higher and tunable SPR absorption in the visible region. However, few potential problems including sensitivity, selectivity and cost

Received: March 8, 2016

Accepted: May 11, 2016

Published: May 11, 2016

have also been reported in the practical implementations of Au-NPs-based mercury sensors.<sup>3,16,20–22</sup> Naked eye visible Ag-NPs are extensively used to alter the emission behavior of dye molecules because of their SPR bands matching with the emission bands of the dyes.<sup>14,23</sup> In addition, fluorescence quenching is one of the most powerful methods used in medical science and material science due to its sensitive and selective information about interaction between a dye and quencher.<sup>13,24</sup> Fluorescence intensity of a fluorophore is quenched upon interaction with quencher through excited state reaction, ground state complexation (static quenching), collisional interaction (dynamic quenching) or energy transfer.<sup>14,24</sup> During the interaction between the dye and the NPs through the process of Förster resonance energy transfer (FRET) or nanosurface energy transfer (NSET), NPs work as an energy acceptor and the dye works as an energy donor.<sup>25,26</sup> There are various methods based on fluorescence/FRET/NSET described in the literature for Hg<sup>2+</sup> detection.<sup>10,13,14,20,23</sup> These are efficient techniques for the determination of Hg<sup>2+</sup>; however, highly selective and ultrasensitive fluorescence-NSET based “turn on” fluorescence mercury sensor are not frequently reported. In addition, some of the fluorescence-NSET based Hg<sup>2+</sup> sensors are not highly selective, i.e., suffer from cross-sensitivity toward other metal ions, particularly Cu<sup>2+</sup>, Mn<sup>2+</sup>, and Pb<sup>2+</sup>, and on the other hand require time-effective, sensitive, and economical operation that is limited due to time-consuming and complex sample preparation with relatively high cost of starting materials.<sup>27–30</sup> In the given context, development of a highly efficient, low cost, ultrasensitive, and highly selective NSET based Hg<sup>2+</sup> sensors for rapid qualitative as well as quantitative analysis of Hg<sup>2+</sup> in real world water samples is the motivation of the present work.

In this work, we report a highly efficient, low cost NSET based ultrasensitive “turn on” fluorescence sensor capable of exhibiting a high selectivity for Hg<sup>2+</sup> ions in the background of a wide range of competing heavy metal ions. This report is devoted to study the steady-state fluorescence quenching of the probe PVA-NPA by Ag-NPs and the interaction between them. “Turn on” fluorescence depends on the interaction between metal NPs (Ag-NPs) and Hg<sup>2+</sup> ions in the solution. Picosecond time-resolved NSET studies on the ligands with the metal NPs confirm the excited-state energy transferred of fluorophores through the nonradiative process to metal NPs. The emission of the fluorescence probe PVA-NPA and Ag-NPs mixture solution is increased following the addition of Hg<sup>2+</sup> ions with a short response time. The possible interaction between Ag-NPs and mercury ions has been examined by TEM imaging studies. To the best of our knowledge, this is the first NSET based ultrasensitive “turn on” fluorescence sensor for Hg<sup>2+</sup> ions detection with very high selectivity even in the presence of other metal ions within aqueous media.

## MATERIALS AND METHODS

**Materials.** In this study, analytical grade chemicals were used as received without further purification for synthesis and sample preparation. Silver nitrate (AgNO<sub>3</sub>, 99.99%), sodium citrate, sodium borohydride, sodium hydroxide, 4-nitrophenylanthranilate (NPA), and poly(vinyl alcohol) (MW 89 000–98 000) (PVA) were purchased from Sigma-Aldrich. Acetonitrile (Merck) was used as a suitable solvent of NPA. All different metal ions, in the form of nitrate or chloride salts, were purchased from chemical companies Merck or Aldrich and used as received without further purification. The stock solutions (50 mM) of all metal ions were prepared by taking a known amount of chloride or nitrate salts in the aqueous medium. Millipore

water was used as aqueous solvent. Groundwater (from S. N. Bose National Centre for Basic Sciences, Kolkata, India) was used as a real water samples.

**Synthesis of Silver Nanoparticles and PVA Capped NPA Solution.** Citrate capped silver nanoparticles were prepared in aqueous solution by following the reported literature.<sup>31</sup> The PVA capped NPA solution was synthesized by mixing aqueous solution of PVA with acetonitrile solution of NPA at a weight ratio of PVA/NPA of 1200:1. The aqueous PVA solution was prepared by dissolving 0.9 g of PVA in 30 mL of water under stirring condition upon heating at temperature around 70 °C. The pH of the solution was adjusted to 7.5 by adding aqueous solution of NaOH. Then 4 mL of 1 mM acetonitrile solution of NPA was prepared at room temperature. A 3 mL aliquot of stock NPA solution was added in a 30 mL PVA aqueous solution at room temperature under stirring condition, in six aliquots with an interval of 30 min. The greenish yellow solution was washed extensively with ethanol (Merck) to remove free NPA and side product. After that, the precipitated PVA capped NPA was dissolved in a 30 mL water. The formation of PVA capped NPA was confirmed by the strong emission band at around 420 nm.

**Procedure for Hg<sup>2+</sup> Ions Detection in Real World Samples.** Groundwater samples were collected from the campus and used as model real world samples. The collected samples were spiked with various known concentration ranges of mercury and filtered using 0.22 μm pore size filters. For sensing, 800 μL of Hg<sup>2+</sup> spiked water samples was taken for the analysis using our developed sensor (final concentrations of mercury in the solution were prepared to be 1 ppb, 1 ppm, and 10 ppm).

**Optical Studies.** Optical absorption of the resulting solution was measured by using Shimadzu UV-2600 spectrophotometer with a quartz cell of 1 cm path length. The extinction coefficient of citrate-capped Ag-NPs at 395 nm of  $5.56 \times 10^8 \text{ M}^{-1} \text{ cm}^{-1}$ , derived from literature,<sup>32</sup> was used to calculate the nanoparticle concentration of the stock samples by using the Beer–Lambert law. We used high-resolution transmission electron microscopy (HRTEM) to characterize the particle size and detailed structural information on NPs. TEM samples were prepared by dropwise addition of the diluted samples on to carbon-coated copper grids. The steady-state emissions were measured with a JobinYvon Fluorolog fluorometer. The emissions of all the samples were taken upon excitation at the wavelength of 340 nm. Time correlated single photon counting (TCSPC) setup from Edinburgh Instruments UK was used to measure picosecond time-resolved fluorescence transients. For 375 nm excitation, we used a picosecond pulsed laser diode with 80 ps instrument response function (IRF). The excitation laser was vertically polarized and the emission was collected through a polarizer oriented at 55° with the vertical position. The picosecond transient fluorescence decays were fitted with multiexponential (n) function,  $\sum_{i=1}^n A_i \exp(-t/\tau_i)$  where, A<sub>i</sub>'s are weight percentages of the decay components with time constants of τ<sub>i</sub>. The average excited state lifetime is expressed by the equation  $\tau_{\text{avg}} = \sum_{i=1}^n A_i \tau_i$ , when  $\sum_{i=1}^n A_i = 1$ .

**Nanosurface Energy Transfer (NSET) Technique.** The technique is well explained in literature.<sup>25,32</sup> The distances of donor–acceptor pair can be easily calculated by using the following equations.

$$k_{\text{et}} = 0.3 \left( \frac{\mu^2 \omega_{\text{dye}}}{\eta \omega_{\text{F}} k_{\text{F}} d^4} \right) \quad (1)$$

Through the use of Einstein A<sub>21</sub> coefficient, eq 1 can be simplified as<sup>33</sup>

$$A_{21} = \frac{\omega_{\text{dye}}^3}{3\epsilon_0 \eta \pi c^3} |\mu^2| \quad (2)$$

The rate of energy transfer in accordance with Coulomb's law  $1/4\pi\epsilon_0$  is expressed as

$$k_{\text{et}} = 0.225 \frac{c^3 \phi_{\text{dye}}}{\omega_{\text{dye}}^2 \omega_{\text{F}} k_{\text{F}} d^4 \tau_{\text{dye}}} \quad (3)$$

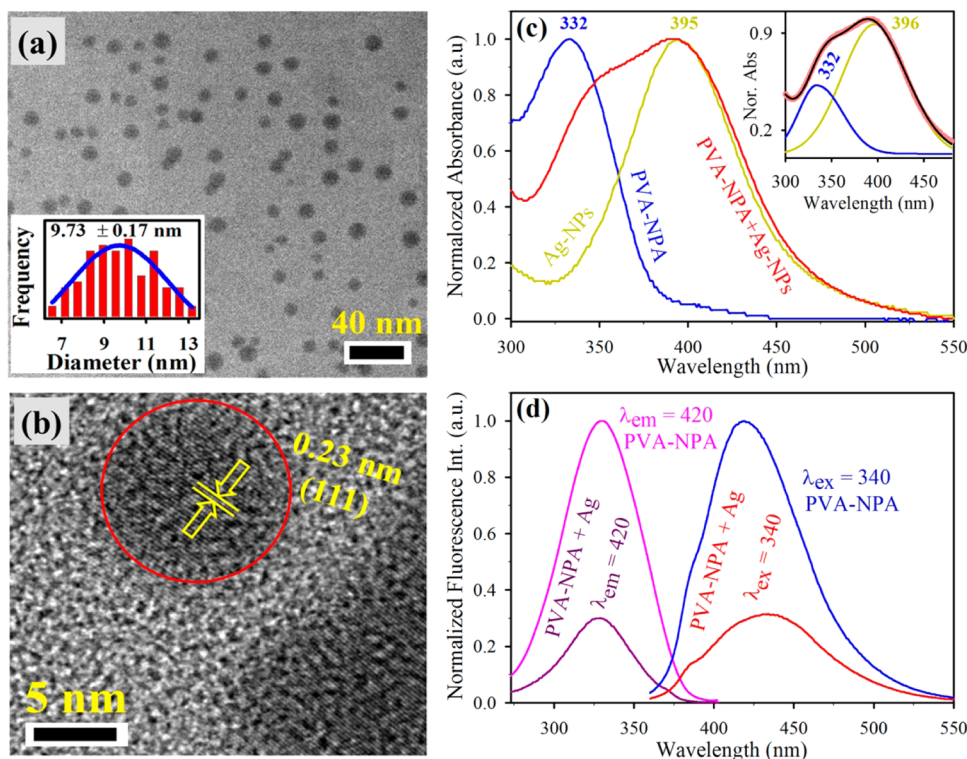


**Figure 1.** (a) TEM images of Ag-NPs with an average diameter of 10 nm. Inset shows the size distribution of the Ag-NPs. (b) High-resolution TEM (HRTEM) image of Ag-NPs. (c) UV–vis absorption spectra of Ag-NPs (deep yellow), PVA-NPA (blue), and PVA-NPA in the presence of Ag-NPs (red). Inset shows the curve deconvolution of PVA-NPA in the presence of Ag-NPs. (d) Steady-state fluorescence emission ( $\lambda_{em} = 420$  nm) and excitation ( $\lambda_{ex} = 340$  nm) spectra of PVA-NPA in the absence and presence of acceptor (Ag-NPs).

where  $c$  is the speed of light and  $\phi_{dye}$  is the quantum yield of the donor is 0.51.<sup>26</sup> The angular frequency ( $\omega_{dye}$ ) for the donor is  $4.48 \times 10^{15} \text{ s}^{-1}$ , and the angular frequency ( $\omega_F$ ) and the Fermi wave vector ( $k_F$ ) for the bulk silver are  $8.3 \times 10^{15} \text{ s}^{-1}$  and  $1.2 \times 10^8 \text{ cm}^{-1}$ , respectively.<sup>34</sup>  $d$  is the donor–acceptor distance. The average lifetime of the dye ( $\tau_{dye}$ ) is 2.3 (ns). The  $d_0$  value is the distance at which a dye exhibits equal probabilities for energy transfer and spontaneous emission. The  $d_0$  value is given by

$$d_0 = \left( 0.225 \frac{c^3 \phi_{dye}}{\omega_{dye}^2 \omega_F k_F} \right)^{1/4} \quad (4)$$

Here, we have used  $k_{et}$  as  $k_{\text{time-resolved}}$

$$k_{\text{time-resolved}} = \frac{1}{\tau_{\text{donor-acceptor}}} - \frac{1}{\tau_{dye}} \quad (5)$$

where  $\tau_{\text{donor-acceptor}}$  is the average donor–acceptor system lifetime.

Now the donor–acceptor distance  $d$  can be calculated by following the given equation

$$d = \frac{d_0}{(k_{et} \tau_{dye})^{1/4}} \quad (6)$$

## RESULTS AND DISCUSSION

**Characterization and Interaction of Ag-NPs with PVA-NPA.** The prepared Ag-NPs were characterized by TEM imaging as well as UV–vis spectra. Figure 1a represents the TEM image of the citrate capped Ag-NPs. The TEM images reveal the spherical particles in shape with almost uniform size distribution. The average diameter of particles has been found to be 10 nm (inset of Figure 1a). The details crystallographic structural information on Ag-NPs was provided by HRTEM.

Figure 1b illustrates the HRTEM image of the NPs, showing continuous single directional lattice fringes. The interplanar distance of the fringes measured to be about 0.23 nm corresponds to the interplanar distance of Ag [111] lattice planes.<sup>35</sup> The UV–vis spectra of prepared Ag-NPs are shown in the Figure 1c (yellow color). The observed characteristic absorbance band peaking at around 395 nm due to SPR band of the Ag-NPs also indicates the formed particle size is around 10 nm.<sup>19</sup> As shown in Figure 1c, the fluorescent dye PVA capped NPA (PVA-NPA) exhibits an absorption band peaking at around 332 nm. In addition to that, the absorption band of PVA-NPA in the presence of Ag-NPs was shifting toward the absorbance maxima of Ag-NPs but the absorbance due to Ag-NPs was unchanged. The absorbance maxima shift may be due to the very strong and broad absorbance of Ag-NPs compared to PVA-NPA in the overlapping region (pseudoshift) or the complex formation between them. The deconvolution of absorbance spectra of PVA-NPA with Ag-NPs (inset of Figure 1c) indicates a pseudoshift in the absorbance band of PVA-NPA in the presence of Ag-NPs. All the absorbance spectra are represented after scattering correction following the reported literature.<sup>36,37</sup> As shown in Figure 1d, the strong emission of PVA-NPA was found at around 420 nm, upon 340 nm excitation. A significant quenching of PVA-NPA emission was observed upon addition of Ag-NPs, keeping fixed the concentration of PVA-NPA in the solution. The Figure 1d also shows the excitation spectra of PVA-NPA and PVA-NPA with Ag-NPs monitored at the emission peak (420 nm). The excitation spectra for both PVA-NPA and PVA-NPA with Ag-NPs show maxima at around 330 nm. In addition, the excitation spectra for PVA-NPA with Ag-NPs also reveal the

pseudo shift which is in accordance to the observations made from the curve deconvolution of absorption spectra.

**Quenching Mechanisms and Titration Study.** Figure 2a represents the steady-state fluorescence quenching of PVA-

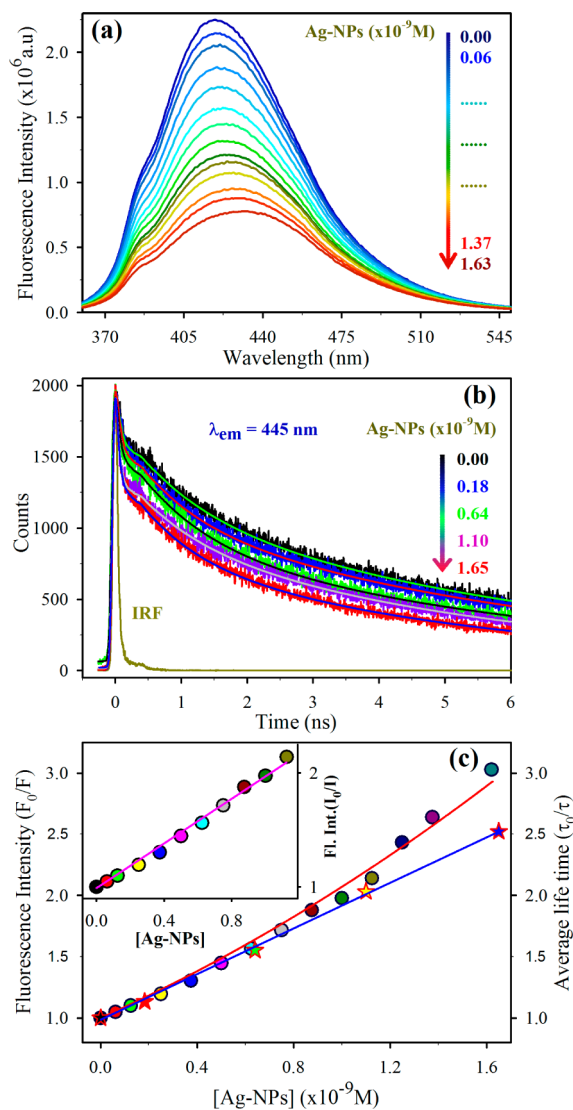


**Figure 2.** (a) Fluorescence emissions spectra ( $\lambda_{\text{ex}} = 340 \text{ nm}$ ) of PVA-NPA with increasing concentrations of Ag-NPs (0.00, 0.06, 0.12, 0.25, 0.37, 0.50, 0.62, 0.75, 0.87, 1.00, 1.13, 1.25, 1.37, and  $1.63 \times 10^{-9} \text{ M}$ ). (b) Picosecond time-resolved fluorescence transients of the donor with increasing concentrations of Ag-NPs (0.00, 0.18, 0.64, 1.10, and  $1.65 \times 10^{-9} \text{ M}$ ), upon excitation at 375 nm. (c) Plots of  $F_0/F$  vs [Ag-NPs] at 420 nm (red) and  $\tau_0/\tau$  vs [Ag-NPs] ( $\lambda_{\text{ex}} = 375 \text{ nm}$ ) (blue). Inset shows the linear part of the plot of  $F_0/F$  vs [Ag-NPs].

NPA in aqueous solution with increasing concentration of Ag-NPs. Upon 340 nm excitation, the maximum emission wavelength of PVA-NPA was at around 420 nm. In addition, the emission peak is shifting toward higher wavelength with increasing concentration of Ag-NPs. The observed peak shift and decrease in fluorescence intensity of PVA-NPA in the presence of Ag-NPs can arise either due to excited state reaction or collisional interaction (dynamic) or static quenching or both or even through nonmolecular mechanisms where fluorophore itself or other absorbing species attenuates the fluorescence intensity.<sup>38</sup>

The specified quenching mechanism can be determined by lifetime measurements. Figure 2b represents the fluorescence transients of PVA-NPA in the absence and presence of different concentrations of Ag-NPs (acceptor) monitored at 445 nm. The fluorescence transients of PVA-NPA exposed multi-exponential time constants with an average lifetime ( $\tau_0$ ) of 2.3 ns as tabulated in Table 1. Furthermore, it has also been observed that the fluorescence transient for the donor–acceptor system the average lifetime ( $\tau$ ) decreases with the increase in Ag-NPs concentration (Table 1) which indicates efficient energy transfer from PVA-NPA donor to Ag-NPs acceptor.

In order to understand the quenching mechanism, the relative change in fluorescence intensity and average lifetime of PVA-NPA has been plotted as a function of the quencher (Ag-NPs) concentration as shown in Figure 2c. For the collisional (dynamic) quenching, the relative change in fluorescence intensity and average lifetime is linearly related to the quencher concentration, as described by the well-known Stern–Volmer (SV) equation.<sup>39</sup>

$$F_0/F = 1 + k_q \tau_0 [Q] = 1 + K_{SV} [Q] \quad (7)$$

and

$$\tau_0/\tau = 1 + k_q \tau_0 [Q] = 1 + K_D [Q] \quad (8)$$

where  $k_q$  is the bimolecular quenching constant,  $\tau_0$  and  $\tau$  are the lifetime of the fluorophore in the absence and present of quencher, respectively,  $[Q]$  is the quencher concentration,  $F_0$  and  $F$  are the fluorescence intensities in the absence and presence of quencher, respectively,  $K_{SV}$  is the Stern–Volmer constant, and  $K_D$  is the dynamic quenching constant. In the case of pure collisional (dynamic) quenching,  $\tau_0/\tau = F_0/F$ , while for static quenching  $F_0/F$  increases but  $\tau$  remains unchanged, i.e.,  $\tau_0/\tau = 1$ .<sup>23,39</sup> As shown in Figure 2c for the quencher concentration below  $1.13 \times 10^{-9} \text{ M}$ , a linear SV plot  $F_0/F$  vs  $[Q]$  (inset of Figure 2c) with almost equal slope value of the plot  $\tau_0/\tau$  vs  $[Q]$  has been observed. The observed results indicate that the quenching mechanism is purely collisional (dynamic) for the quencher (Ag-NPs) concentration lower than  $1.13 \times 10^{-9} \text{ M}$ . Then it is possible to estimate the dynamic quenching constant ( $K_D$ ) and the Stern–Volmer constant

**Table 1.** Dynamics of Picosecond Time-Resolved Fluorescence Transients of PVA-NPA in the Absence and Presence of Different Concentrations of Ag-NPs (acceptor), Monitored at 445 nm

figure	samples	Ag-NPs concn	$\tau_1$ (ps)	$\tau_2$ (ns)	$\tau_3$ (ns)	$\tau_{\text{avg}}$ (ns)
Figure 2b	PVA-NPA	0.00	54 (53.4%)	1.0 (16.0%)	6.9 (30.5%)	2.3
	PVA-NPA + Ag-NPs	$0.55 \times 10^{-9} \text{ M}$	48 (56.4%)	0.9 (15.7%)	6.6 (27.9%)	2.0
		$1.90 \times 10^{-9} \text{ M}$	42 (60.4%)	1.0 (16.9%)	5.7 (22.7%)	1.5
		$3.30 \times 10^{-9} \text{ M}$	32 (72.6%)	1.0 (9.4%)	5.6 (18.0%)	1.1
		$4.95 \times 10^{-9} \text{ M}$	30 (73.3%)	0.8 (11.3%)	5.1 (15.4%)	0.9

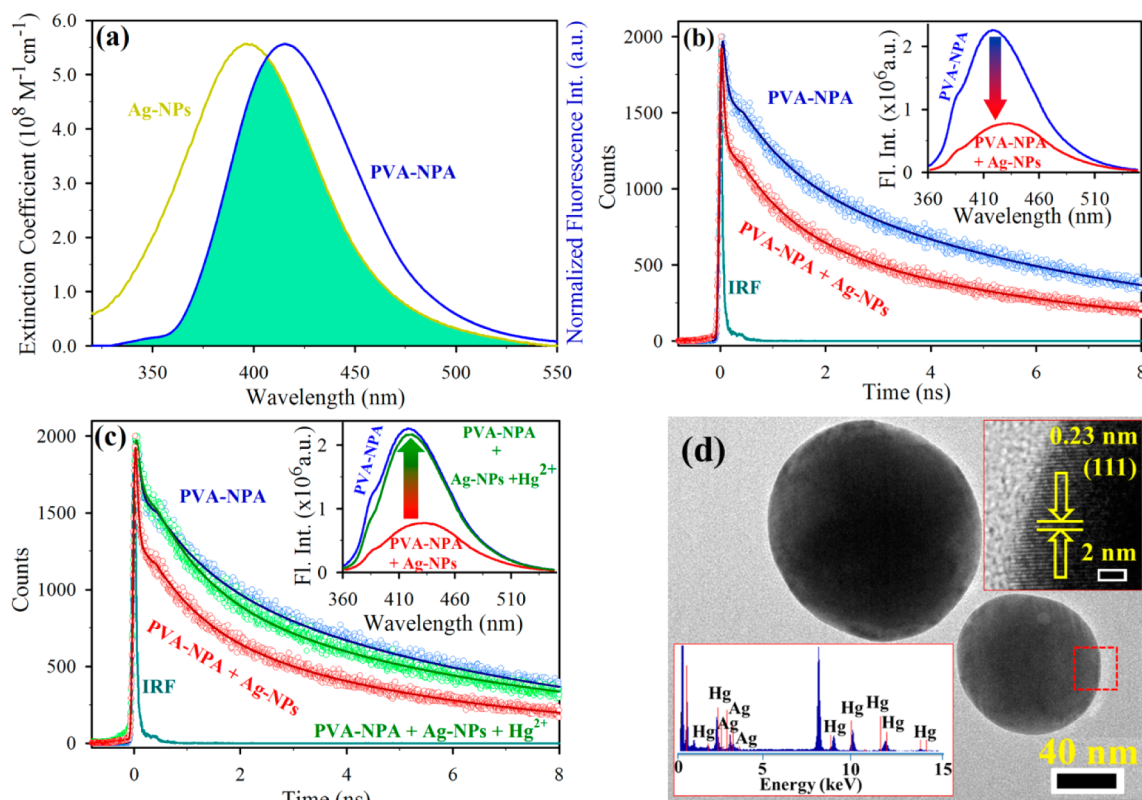


**Figure 3.** (a) Spectral overlap between emission spectrum of donor (PVA-NPA) and the absorption spectrum of acceptor (Ag-NPs). (b) Picosecond time-resolved fluorescence transients of donor in the absence and presence of the acceptor, monitored at  $\lambda_{em} = 445$  nm. Inset shows corresponding fluorescence emissions spectra ( $\lambda_{ex} = 340$  nm). (c) Picosecond time-resolved fluorescence transients of the PVA-NPA + Ag-NPs complex upon interaction with  $Hg^{2+}$  metal ions, monitored at  $\lambda_{em} = 445$  nm. Inset shows corresponding fluorescence emissions spectra ( $\lambda_{ex} = 340$  nm). (d) TEM image of the complex PVA-NPA + Ag-NPs after interaction with  $Hg^{2+}$  ions. Upper inset shows the HRTEM image obtained from the highlighted (red square) region and lower inset shows the EDAX spectra.

**Table 2. Dynamics of Picosecond Time-Resolved Fluorescence Transients of PVA-NPA, PVA-NPA + Ag-NPs, and PVA-NPA + Ag-NPs +  $Hg^{2+}$ , Monitored at 445 nm**

figure	samples	$\tau_1$ (ps)	$\tau_2$ (ns)	$\tau_3$ (ns)	$\tau_{avg}$ (ns)
Figures 2b and 3c	PVA-NPA	54 (53.4%)	1.0 (16.0%)	6.9 (30.5%)	2.3
	PVA-NPA + Ag-NPs	30 (73.3%)	0.8 (11.3%)	5.1 (15.4%)	0.9
	PVA-NPA + Ag-NPs + $Hg^{2+}$	54 (49.4%)	1.0 (23.5%)	6.7 (27.1%)	2.1

( $K_{SV}$ ) based on eqs 7 and 8. It turns out that  $K_{SV}$  and  $K_D$  are equal to  $0.98 \times 10^9$  and  $0.93 \times 10^9 M^{-1}$ , respectively. Now, in the case of higher concentrations of Ag-NPs, the nonlinear upward curvature SV plot (Figure 2c) suggests that maybe both dynamic and static quenching mechanisms are occurring. When both static and dynamic quenching mechanisms occur, the SV equation gets modified as<sup>39</sup>

$$F_0/F = (1 + k_q\tau_0[Q])(1 + K_S[Q]) \quad (9)$$

where  $K_S$  represents the static quenching constant. In such a case, the plot  $F_0/F$  vs  $[Q]$  will have an upward curvature due to the  $[Q]^2$  term, which accounts for the upward curvature in our SV plots shown in Figure 2c.

**FRET and NSET Studies.** In order to rationalize the above quenching phenomena, picosecond resolved fluorescence spectroscopy was performed. As shown in Figure 3a, a huge spectral overlap (overlap integral value  $[J(\lambda)]$  is equal to  $1.06 \times 10^{19} M^{-1} cm^{-1} nm^4$ ) between the emission spectrum of PVA-NPA and absorption spectrum of Ag-NPs makes these two entities excellent donor–acceptor pairs, suggesting an efficient

energy transfer (ET) between them. To confirm the resonance type of energy transfer from PVA-NPA to Ag-NPs, a picosecond resolved fluorescence study was monitored at 445 nm upon excitation at 375 nm wavelength. The inset of Figure 3b represents the steady-state fluorescence spectra of PVA-NPA in the absence and presence of Ag-NPs that indicates the energy transfer occurs between the donor and acceptor. For further confirmation, we measured the excited state lifetime of PVA-NPA with and without Ag-NPs as shown in Figure 3b. The time constants of the fluorescence transients at 445 nm for PVA-NPA and PVA-NPA with Ag-NPs revealed multi-exponential decay, with an average lifetime of 2.3 and 0.90 ns, respectively. The details of the lifetime components of the transients are tabulated in Table 2. A significant faster component observed in donor–acceptor system which indicates efficient ET occurs from PVA-NPA to Ag-NPs. Upon utilization of the FRET scheme<sup>32</sup> the donor–acceptor distance was found to be 18.13 nm. As the calculated donor–acceptor distance exceeds 100 Å, the appropriate model for our system is NSET, which typically occurs if donors are located

too close to acceptors surface.<sup>34</sup> In order to approve the NSET model, the distance between donor and acceptor is determined to be 5.66 nm ( $d_0 = 6.27$  nm) from eqs 6 and 4, respectively. Herein, we propose NSET from the donor PVA-NPA to the acceptor Ag-NPs, as the measured donor–acceptor distance is comparable to the radius ( $\sim 5$  nm) of the silver NPs. Hence, it is worth emphasizing that the energy transfers from PVA-NPA to Ag-NPs results in the quenching of PVA-NPA emission.

**Sensing Mechanism for Detection of  $\text{Hg}^{2+}$  Ions.** In order to understand, how the quenching phenomena as well as lifetime of the dye are affected by the metal  $\text{Hg}^{2+}$  ions, we furthermore performed the picosecond resolved fluorescence transients at 445 nm for the quenched system in the presence of  $\text{Hg}^{2+}$  ions. The inset of Figure 3c shows the drastic emissions of the quenched system in the presence of  $\text{Hg}^{2+}$  ions, which are almost same as the emissions of the PVA-NPA system, which indicates no energy transfer occurs between the donor (PVA-NPA) and acceptor (Ag-NPs) in the presence of  $\text{Hg}^{2+}$  ions. For more confirmation, we present the fluorescence transient spectra in Figure 3c, which shows the decay lifetime of the donor–acceptor system in the presence of  $\text{Hg}^{2+}$  ions is similar to that in the PVA-NPA system. The detailed lifetime components of the transients are tabulated in Table 2. The observed result indicates “turn on” fluorescence as well as “turn off” NSET that is deactivation of NSET phenomena are occurring in the presence of  $\text{Hg}^{2+}$  ions. This “on–off” phenomenon is happening in the presence of  $\text{Hg}^{2+}$  ions due to the aggregation<sup>40,41</sup> of metal NPs as well as the amalgam formation of Ag-NPs with  $\text{Hg}^{2+}$  ions.<sup>11,42,43</sup> The amalgam formed by reduction of  $\text{Hg}^{2+}$  in the presence of silver nanoparticles.<sup>11,44,45</sup> Silver nanoparticles reduce  $\text{Hg}^{2+}$  to form the amalgam at the surface of the nanoparticles within the polymer matrix. The oxidation state of the Ag-nanoparticles is also reported to be changed (from 0 to +1) at the surface, leading to significant reduction and blue shifting of the SPR band (reduction of effective sizes of the Ag-NPs upon  $\text{Hg}^{2+}$  amalgamation), imparting remarkable selectivity for the sensing response. As such reactions do not occur with the majority of other transition metal ions, high selectivity is expected. In addition to that, in the time of amalgamation, the Ag-NPs lead to aggregation, leaving free the PVA-NPA dye. Due to aggregation, Ag-NPs lose SPR band and increase the particles size, and as a result the donor–acceptor system behaves like a PVA-NPA system. The aggregation of metal NPs as well as the amalgam formation of Ag-NPs with Hg are further confirmed by the TEM image and EDAX spectra as shown in Figure 3d and the lower inset. The HRTEM image obtained from the square part of the aggregated Ag-NPs, shown in the upper inset of Figure 3d. The continuous single directional lattice fringe with measured interplanar distance of about 0.23 nm corresponds to the interplanar distance of Ag [111] lattice planes. The observed result confirms the aggregation of Ag-NPs as well as the amalgam formation of Ag-NPs with Hg.

**Factors Affecting the Sensing of  $\text{Hg}^{2+}$  ions.** For better analytical performance and in order to obtain a highly sensitive sensor, the experimental conditions were optimized. We first studied the concentration effects of PVA-NPA and Ag-NPs on  $\text{Hg}^{2+}$  sensing. Three different concentration of as prepared PVA-NPA, likely 10%, 20% and 30% (V/V) were employed for the quenching and titration study with increasing concentration of Ag-NPs. Although the normalized fluorescence intensity ( $F_0/F$ ) increased with the increase in Ag-NPs concentration but it was independent of PVA-NPA concentration. So, it is obvious

that the as prepared PVA-NPA concentration will not affect the detection sensitivity significantly. Linear dependency between the normalized fluorescence intensity ( $F_0/F$ ) and Ag-NPs concentration (below  $1.13 \times 10^{-9}$  M) has also been observed (Figure 2c, inset). So, the preferable concentrations for sensing application should be equal or less than  $1.13 \times 10^{-9}$  M Ag-NPs at 20% (V/V) as prepared PVA-NPA. The effects of pH on the sensing was then investigated. We observed that the normalized fluorescence intensity ( $F_0/F$ ) of as prepared sample with pH = 6.5 was weaker at acidic or basic conditions. So as prepared sample (pH = 6.5) is chosen for sensing application. Finally, the response time was studied. We observed that the interaction of the Ag-NPs and  $\text{Hg}^{2+}$  is very fast, which can reach a steady condition within 2 min. This result indicates that the present method is time-saving.

**Selectivity Studies.** It is proved that the synthesized PVA-NPA exhibits a strong emission and quenched by Ag-NPs. After addition of  $\text{Hg}^{2+}$  ions to the quenched solution (final Hg concentration in the solution is 100 ppm), the emission of the solution dramatically increased within a minute and exhibits the same emission as PVA-NPA (as shown in inset of the Figure 3c). Now to investigate the response of our sensor to others metal ions, including  $\text{Cu}^{2+}$ ,  $\text{Cd}^{2+}$ ,  $\text{Ca}^{2+}$ ,  $\text{Co}^{2+}$ ,  $\text{Mg}^{2+}$ ,  $\text{Na}^+$ ,  $\text{K}^+$ ,  $\text{Pb}^{2+}$ ,  $\text{Ni}^{2+}$ ,  $\text{Zn}^{2+}$ , and  $\text{Fe}^{3+}$  were examined under same condition. First, the same concentration (final metal ions concentration in the solution is 100 ppm) of the stock solutions of the as prepared various metals ions were added into sample solution (PVA-NPA + Ag-NPs). These results demonstrate that no significant change in fluorescence intensity in the presence of other metal ions (as indicated in Figure 4). Second, all metal ions (including  $\text{Hg}^{2+}$  and excluding  $\text{Hg}^{2+}$ ) with same concentration were mixed together to form a mixture solution and added into sample solution (PVA-NPA + Ag-NPs) for interference testing. Inset of the Figure 4b reveals the dramatic

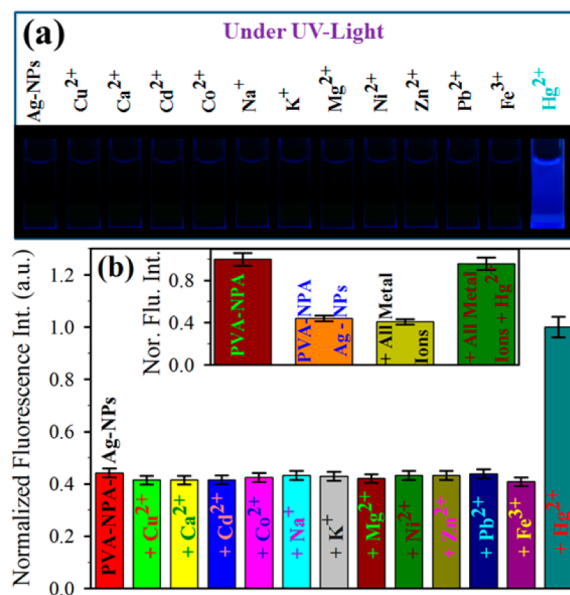


**Figure 4.** (a) Visual representation of PVA-NPA + Ag-NPs complexes upon interaction with metal ions under UV light. (b) Relative fluorescence intensity of the quenched fluorophore (PVA-NPA + Ag-NPs) in the presence of various metal ions (with same concentration) monitored at 433 nm. Inset shows the relative fluorescence intensity of fluorophore and the quenched fluorophore with all metal (except  $\text{Hg}^{2+}$ ) ions in absent and present of  $\text{Hg}^{2+}$  ions.

change in fluorescence intensity occurs only when  $\text{Hg}^{2+}$ -mixed solution was added. The selectivity studies clearly exhibited the high selectivity of our sensor (PVA-NPA + Ag-NPs) to  $\text{Hg}^{2+}$  ions in comparison to other metal ions. The observed result indicated the potential applications of our method for the detection of  $\text{Hg}^{2+}$  ions in aqueous medium without any interference of other metal ions.

**Sensitivity Studies.** The sensing and optical properties of the sensor were investigated by various measurements. In this subsection, we are demonstrating the qualitative as well as quantitative detection of mercury ions in aqueous medium by our ultrasensitive sensor. Figure 5a reveals “turn on” fluorescence signal instantly upon addition of  $\text{Hg}^{2+}$  ions into the sensor (aqueous PVA-NPA with Ag-NPs) and intensity increased as the concentration of  $\text{Hg}^{2+}$  ions increased in a dynamic range that spanned 0–40 ppm. Meanwhile, the yellow solution rapidly became colorless and a blue shift was observed in the spectra due to decreasing concentration and the aggregation of the nanoparticles. Inset of Figure 5a shows that our highly efficient and ultrasensitive sensor had a detection limit of 100 ppt (0.5 nM) for  $\text{Hg}^{2+}$  ions, which was in the same range or at a lower value compared to recently reported colorimetric as well as fluorescence and energy transfer base sensor.<sup>13,20,46–53</sup> Upper inset of Figure 5b exhibits the linear response (with slope = 0.086) of the sensor for very low concentration (0–1 ppb) of  $\text{Hg}^{2+}$  ions. For high concentration (1 ppb to 40 ppm) of  $\text{Hg}^{2+}$  ions, the sensor follows nonlinearity by the equation  $Y = (0.916 - 0.004X^{0.4})^{-1}$ , where  $Y$  is the normalized fluorescence intensity and  $X$  (in ppb) is the  $\text{Hg}^{2+}$  ions concentration (shown in the lower inset of the Figure 5b). These results imply that this highly selective, cost-effective, and ultrasensitive novel sensor can be applied to the direct detection of  $\text{Hg}^{2+}$  ions in real world water samples as well as drinking water.

#### Determination of $\text{Hg}^{2+}$ Ions in Real World Samples.

Application of our proposed method has been evaluated for the determination of  $\text{Hg}^{2+}$  in a real world samples. We choose groundwater as a real sample. In such environmental samples, the concentration of other metal ions and some unknown contamination are significantly higher than that of  $\text{Hg}^{2+}$  ions, so it is highly challenging to detect mercury in real world samples. Figure 5c represents the comparative analysis between the value obtained from calibration curve and instrumental data for different concentration of  $\text{Hg}^{2+}$  contaminated groundwater. It has been found that the real world sample was free from  $\text{Hg}^{2+}$  ions contaminations. Upon addition of the  $\text{Hg}^{2+}$  ions contamination in the water samples with various known concentrations, it has been observed that the value obtained from the calibration curve and the values measured were within the 10% error range. This result suggests that the proposed sensor has potential for sensing of  $\text{Hg}^{2+}$  ions in environmental real world samples.

## CONCLUSION

In summary, the quenching of dye fluorescence by Ag-NPs was studied using fluorescence spectroscopy. The quenching process was characterized by well-known Stern–Volmer plots which display a dynamic quenching for the quencher concentration below  $1.13 \times 10^{-9}$  M. The calculated donor–acceptor distance ( $d = 5.66$  nm) by NSET model confirmed the energy transfer phenomenon between the fluorescent dye and NPs. The present study demonstrates the unique potential of metal nanoparticle in chemical sensing application followed by

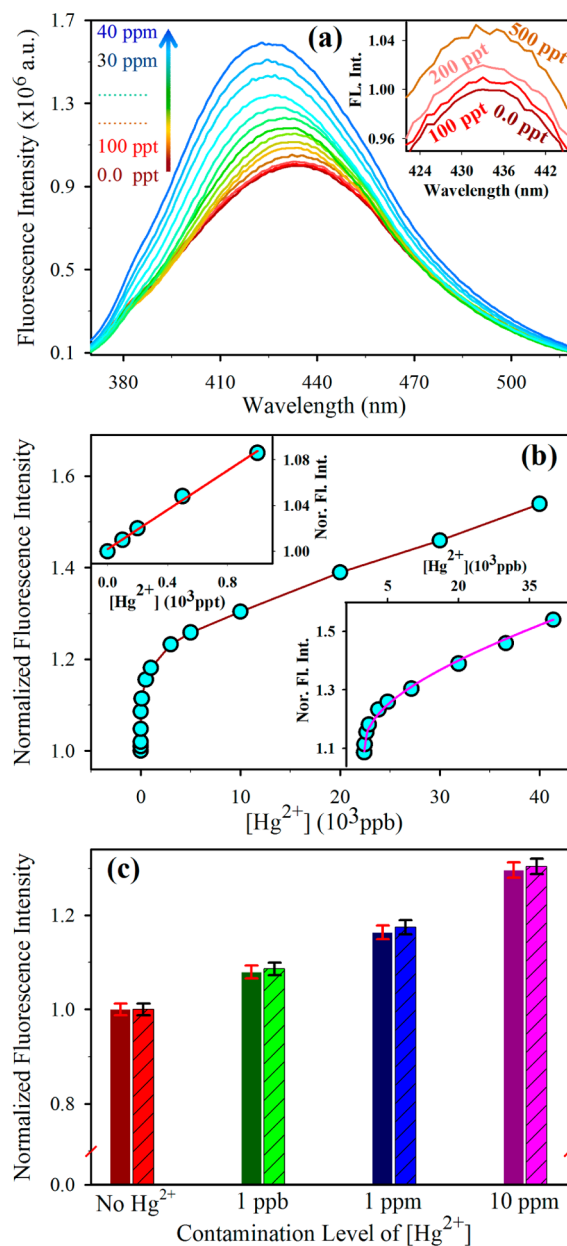


**Figure 5.** (a) Steady-state fluorescence spectra ( $\lambda_{\text{ex}} = 340$  nm) of the quenched fluorophore (PVA-NPA + Ag-NPs) upon addition of  $\text{Hg}^{2+}$  ions (0–40 ppm). Inset shows the magnified fluorescence spectra for some low concentration (0, 100, 200, and 500 ppt) of  $\text{Hg}^{2+}$  ions. (b) The plot of normalized fluorescence intensity vs  $[\text{Hg}^{2+}]$ , at 433 nm. Upper inset shows the linear response with  $[\text{Hg}^{2+}]$  from 0 to 1 ppb, and the lower inset shows the nonlinear response with  $[\text{Hg}^{2+}]$  from 1 ppb to 40 ppm. (c) Response of the sensor without and with contaminated real water samples, and comparison of measured values (solid bars) with proposed values (cross bars).

the nonradiative energy transfer process. We have successfully developed a very low cost, highly selective, and ultrasensitive “turn on” fluorescence sensor based on NSET for direct detection of  $\text{Hg}^{2+}$  in aqueous medium with the detection limit 100 ppt (0.5 nM). The developed sensor is not only insensitive to other metal ions but also highly selective toward  $\text{Hg}^{2+}$  ions in the presence of other metal ions. The developed sensor has potential applications in monitoring trace  $\text{Hg}^{2+}$  ions in real world samples. The scope for further development of this

concept is extensive, which offers great potential for the development of economical portable devices.

## AUTHOR INFORMATION

### Corresponding Author

\*E-mail: [skpal@bose.res.in](mailto:skpal@bose.res.in) (S.K.P.).

### Notes

The authors declare no competing financial interest.

## ACKNOWLEDGMENTS

P.K.S. is thankful to UGC, India for providing the fellowship under the UGC-RGNF scheme, and N.P. acknowledges DST (India) for INSPIRE Fellowship. We are thankful to DAE (India) for Financial Grant 2013/37P/73/BRNS, DST (India) for Financial Grant SB/S1/PC-011/2013, NTH-School "Contacts in Nanosystems: Interactions, Control and Quantum Dynamics", the Braunschweig International Graduate School of Metrology (IGSM), and DFG-RTG 1952/1, Metrology for Complex Nanosystems.

## REFERENCES

- (1) Wang, Q.; Kim, D.; Dionysiou, D. D.; Sorial, G. A.; Timberlake, D. Sources and remediation for mercury contamination in aquatic systems—a literature review. *Environ. Pollut.* **2004**, *131* (2), 323–336.
- (2) Eisler, R. Health risks of gold miners: a synoptic review. *Environ. Geochem. Health* **2003**, *25* (3), 325–345.
- (3) Wang, H.; Wang, Y.; Jin, J.; Yang, R. Gold Nanoparticle-Based Colorimetric and "Turn-On" Fluorescent Probe for Mercury(II) Ions in Aqueous Solution. *Anal. Chem.* **2008**, *80* (23), 9021–9028.
- (4) Ke, J.; Li, X.; Zhao, Q.; Hou, Y.; Chen, J. Ultrasensitive Quantum Dot Fluorescence quenching Assay for Selective Detection of Mercury Ions in Drinking Water. *Sci. Rep.* **2014**, *4*, 5624.
- (5) Miller, J. R.; Rowland, J.; Lechler, P. J.; Desilets, M.; Hsu, L.-C. Dispersal of mercury-contaminated sediments by geomorphic processes, Sixmile Canyon, Nevada, USA: implications to site characterization and remediation of fluvial environments. *Water, Air, Soil Pollut.* **1996**, *86* (1–4), 373–388.
- (6) Tchounwou, P. B.; Ayensu, W. K.; Ninashvili, N.; Sutton, D. Review: Environmental exposure to mercury and its toxicopathologic implications for public health. *Environ. Toxicol.* **2003**, *18* (3), 149–175.
- (7) Farhadi, K.; Forough, M.; Molaei, R.; Hajizadeh, S.; Rafipour, A. Highly selective Hg<sup>2+</sup> colorimetric sensor using green synthesized and unmodified silver nanoparticles. *Sens. Actuators, B* **2012**, *161* (1), 880–885.
- (8) Baughman, T. A. Elemental mercury spills. *Environ. Health Perspect.* **2006**, *114*, 147–152.
- (9) Butler, O. T.; Cook, J. M.; Harrington, C. F.; Hill, S. J.; Rieuwerts, J.; Miles, D. L. Atomic spectrometry update. Environmental analysis. *J. Anal. At. Spectrom.* **2006**, *21* (2), 217–243.
- (10) Nolan, E. M.; Lippard, S. J. Tools and Tactics for the Optical Detection of Mercuric Ion. *Chem. Rev.* **2008**, *108* (9), 3443–3480.
- (11) Ramesh, G. V.; Radhakrishnan, T. P. A Universal Sensor for Mercury (Hg, HgI, HgII) Based on Silver Nanoparticle-Embedded Polymer Thin Film. *ACS Appl. Mater. Interfaces* **2011**, *3* (4), 988–994.
- (12) Wan, Y.; Niu, W.; Behof, W. J.; Wang, Y.; Boyle, P.; Gorman, C. B. Aminoisoquinolines as colorimetric Hg<sup>2+</sup> sensors: the importance of molecular structure and sacrificial base. *Tetrahedron* **2009**, *65* (22), 4293–4297.
- (13) Wanichacheva, N.; Hanmeng, O.; Kraithong, S.; Sukrat, K. Dual optical Hg<sup>2+</sup>-selective sensing through FRET system of fluorescein and rhodamine B fluorophores. *J. Photochem. Photobiol., A* **2014**, *278*, 75–81.
- (14) Rezanejad Bardajee, G.; Hooshyar, Z.; Khanjari, M. Dye fluorescence quenching by newly synthesized silver nanoparticles. *J. Photochem. Photobiol., A* **2014**, *276*, 113–121.
- (15) Horimoto, N. N.; Imura, K.; Okamoto, H. Dye fluorescence enhancement and quenching by gold nanoparticles: Direct near-field microscopic observation of shape dependence. *Chem. Phys. Lett.* **2008**, *467* (1–3), 105–109.
- (16) Annadhasan, M.; Muthukumarasamyvel, T.; Sankar Babu, V. R.; Rajendiran, N. Green Synthesized Silver and Gold Nanoparticles for Colorimetric Detection of Hg<sup>2+</sup>, Pb<sup>2+</sup>, and Mn<sup>2+</sup> in Aqueous Medium. *ACS Sustainable Chem. Eng.* **2014**, *2* (4), 887–896.
- (17) Kelly, K. L.; Coronado, E.; Zhao, L. L.; Schatz, G. C. The Optical Properties of Metal Nanoparticles: The Influence of Size, Shape, and Dielectric Environment. *J. Phys. Chem. B* **2003**, *107* (3), 668–677.
- (18) Thompson, D. G.; Stokes, R. J.; Martin, R. W.; Lundahl, P. J.; Faulds, K.; Graham, D. Synthesis of Unique Nanostructures with Novel Optical Properties Using Oligonucleotide Mixed–Metal Nanoparticle Conjugates. *Small* **2008**, *4* (8), 1054–1057.
- (19) Paramelle, D.; Sadovoy, A.; Gorelik, S.; Free, P.; Hopley, J.; Fernig, D. G. A rapid method to estimate the concentration of citrate capped silver nanoparticles from UV-visible light spectra. *Analyst* **2014**, *139* (19), 4855–4861.
- (20) Li, M.; Wang, Q.; Shi, X.; Hornak, L. A.; Wu, N. Detection of Mercury(II) by Quantum Dot/DNA/Gold Nanoparticle Ensemble Based Nanosensor Via Nanometal Surface Energy Transfer. *Anal. Chem.* **2011**, *83* (18), 7061–7065.
- (21) Wang, Z.; Heon Lee, J.; Lu, Y. Highly sensitive "turn-on" fluorescent sensor for Hg<sup>2+</sup> in aqueous solution based on structure-switching DNA. *Chem. Commun.* **2008**, *45*, 6005–6007.
- (22) Guo, L.; Xu, Y.; Ferhan, A. R.; Chen, G.; Kim, D.-H. Oriented Gold Nanoparticle Aggregation for Colorimetric Sensors with Surprisingly High Analytical Figures of Merit. *J. Am. Chem. Soc.* **2013**, *135* (33), 12338–12345.
- (23) Lee, I. Y. S.; Suzuki, H. Quenching dynamics promoted by silver nanoparticles. *J. Photochem. Photobiol., A* **2008**, *195* (2–3), 254–260.
- (24) Webber, S. The Role of Time-Dependent Measurements in Elucidating Static Versus Dynamic Quenching Processes. *Photochem. Photobiol.* **1997**, *65* (1), 33–38.
- (25) Chaudhuri, S.; Sardar, S.; Bagchi, D.; Singha, S. S.; Lemmens, P.; Pal, S. K. Sensitization of an Endogenous Photosensitizer: Electronic Spectroscopy of Riboflavin in the Proximity of Semiconductor, Insulator, and Metal Nanoparticles. *J. Phys. Chem. A* **2015**, *119* (18), 4162–4169.
- (26) Giri, A.; Makhil, A.; Ghosh, B.; Raychaudhuri, A. K.; Pal, S. K. Functionalization of Manganite nanoparticles and their interaction with biologically relevant small ligands: Picosecond time-resolved FRET studies. *Nanoscale* **2010**, *2* (12), 2704–2709.
- (27) Biswal, B.; Bag, B. Preferences of rhodamine coupled (aminoalkyl)-piperazine probes towards Hg(II) ion and their FRET mediated signaling. *Org. Biomol. Chem.* **2013**, *11* (30), 4975–4992.
- (28) Liu, Z.; Zhu, Z.; Wu, Q.; Hu, S.; Zheng, H. Dielectric barrier discharge-plasma induced vaporization and its application to the determination of mercury by atomic fluorescence spectrometry. *Analyst* **2011**, *136* (21), 4539–4544.
- (29) Lee, Y. H.; Lee, M. H.; Zhang, J. F.; Kim, J. S. Pyrene Excimer-Based Calix[4]arene FRET Chemosensor for Mercury(II). *J. Org. Chem.* **2010**, *75* (21), 7159–7165.
- (30) Pang, Y.; Rong, Z.; Xiao, R.; Wang, S. "Turn on" and label-free core–shell Ag@SiO<sub>2</sub> nanoparticles-based metal-enhanced fluorescent (MEF) aptasensor for Hg<sup>2+</sup>. *Sci. Rep.* **2015**, *5*, 9451.
- (31) Flores, C. Y.; Diaz, C.; Rubert, A.; Benítez, G. A.; Moreno, M. S.; Fernández Lorenzo de Mele, M. A.; Salvarezza, R. C.; Schilardi, P. L.; Vericat, C. Spontaneous adsorption of silver nanoparticles on Ti/TiO<sub>2</sub> surfaces. Antibacterial effect on *Pseudomonas aeruginosa*. *J. Colloid Interface Sci.* **2010**, *350* (2), 402–408.
- (32) Muhammed, M. A. H.; Shaw, A. K.; Pal, S. K.; Pradeep, T. Quantum Clusters of Gold Exhibiting FRET. *J. Phys. Chem. C* **2008**, *112* (37), 14324–14330.
- (33) Craig, D. P.; Thirunamachandran, T. *Molecular quantum electrodynamics: an introduction to radiation-molecule interactions*; Courier Corporation: North Chelmsford, MA, 1998.

(34) Kim, K.-S.; Kim, H.; Kim, J.-H.; Kim, J.-H.; Lee, C.-L.; Laquai, F.; Yoo, S. I.; Sohn, B.-H. Correlation of micellar structures with surface-plasmon-coupled fluorescence in a strategy for fluorescence enhancement. *J. Mater. Chem.* **2012**, *22* (47), 24727–24733.

(35) Rodriguez-Leon, E.; Iniguez-Palomares, R.; Navarro, R.; Herrera-Urbina, R.; Tanori, J.; Iniguez-Palomares, C.; Maldonado, A. Synthesis of silver nanoparticles using reducing agents obtained from natural sources (*Rumex hymenosepalus* extracts). *Nanoscale Res. Lett.* **2013**, *8* (1), 318.

(36) Leach, S. J.; Scheraga, H. A. Effect of Light Scattering on Ultraviolet Difference Spectral. *J. Am. Chem. Soc.* **1960**, *82* (18), 4790–4792.

(37) Gratton, E. Method for the automatic correction of scattering in absorption spectra by using the integrating sphere. *Biopolymers* **1971**, *10* (12), 2629–2634.

(38) Banerjee, S.; Sarkar, S.; Lakshman, K.; Dutta, J.; Pal, S. K. UVA Radiation Induced Ultrafast Electron Transfer from a Food Carcinogen Benzo[a]pyrene to Organic Molecules, Biological Macromolecules, and Inorganic Nano Structures. *J. Phys. Chem. B* **2013**, *117* (14), 3726–3737.

(39) Lakowicz, J. R. *Principles of fluorescence spectroscopy*; Springer Science & Business Media: Berlin, 2013.

(40) Wang, Y.; Yang, F.; Yang, X. Colorimetric Detection of Mercury(II) Ion Using Unmodified Silver Nanoparticles and Mercury-Specific Oligonucleotides. *ACS Appl. Mater. Interfaces* **2010**, *2* (2), 339–342.

(41) Li, L.; Gui, L.; Li, W. A colorimetric silver nanoparticle-based assay for Hg (II) using lysine as a particle-linking reagent. *Microchim. Acta* **2015**, *182* (11–12), 1977–1981.

(42) Wu, L. P.; Zhao, H. W.; Qin, Z. H.; Zhao, X. Y.; Pu, W. D. Highly selective Hg (II) ion detection based on linear blue-shift of the maximum absorption wavelength of silver nanoparticles. *J. Anal. Methods Chem.* **2012**, *2012*, 1.

(43) Rex, M.; Hernandez, F. E.; Campiglia, A. D. Pushing the Limits of Mercury Sensors with Gold Nanorods. *Anal. Chem.* **2006**, *78* (2), 445–451.

(44) Katsikas, L.; Gutiérrez, M.; Henglein, A. Bimetallic Colloids: Silver and Mercury. *J. Phys. Chem.* **1996**, *100* (27), 11203–11206.

(45) Henglein, A.; Brancewicz, C. Absorption Spectra and Reactions of Colloidal Bimetallic Nanoparticles Containing Mercury. *Chem. Mater.* **1997**, *9* (10), 2164–2167.

(46) Long, F.; Zhu, A.; Shi, H.; Wang, H.; Liu, J. Rapid on-site/in-situ detection of heavy metal ions in environmental water using a structure-switching DNA optical biosensor. *Sci. Rep.* **2013**, *3*, 2308.

(47) Othman, A. B.; Lee, J. W.; Wu, J.-S.; Kim, J. S.; Abidi, R.; Thuéry, P.; Strub, J. M.; Van Dorsselaer, A.; Vicens, J. Calix[4]arene-Based, Hg<sup>2+</sup>-Induced Intramolecular Fluorescence Resonance Energy Transfer Chemosensor. *J. Org. Chem.* **2007**, *72* (20), 7634–7640.

(48) Ahamed, B. N.; Ghosh, P. An integrated system of pyrene and rhodamine-6G for selective colorimetric and fluorometric sensing of mercury(II). *Inorg. Chim. Acta* **2011**, *372* (1), 100–107.

(49) Liu, Y.; Lv, X.; Zhao, Y.; Chen, M.; Liu, J.; Wang, P.; Guo, W. A naphthalimide–rhodamine ratiometric fluorescent probe for Hg<sup>2+</sup> based on fluorescence resonance energy transfer. *Dyes Pigm.* **2012**, *92* (3), 909–915.

(50) Wang, L.; Yao, T.; Shi, S.; Cao, Y.; Sun, W. A label-free fluorescent probe for Hg<sup>2+</sup> and biothiols based on graphene oxide and Ru-complex. *Sci. Rep.* **2014**, *4*, 5320.

(51) Zhang, H.; Xia, Y. Ratiometry, Wavelength, and Intensity: Triple Signal Readout for Colorimetric Sensing of Mercury Ions by Plasmonic Cu<sub>2</sub>-xSe Nanoparticles. *ACS Sens.* **2016**, *1*, 384.

(52) Zou, Q.; Tian, H. Chemodosimeters for mercury(II) and methylmercury(I) based on 2,1,3-benzothiadiazole. *Sens. Actuators, B* **2010**, *149* (1), 20–27.

(53) Zhou, G.; Chang, J.; Pu, H.; Shi, K.; Mao, S.; Sui, X.; Ren, R.; Cui, S.; Chen, J. Ultrasensitive Mercury Ion Detection Using DNA-Functionalized Molybdenum Disulfide Nanosheet/Gold Nanoparticle Hybrid Field-Effect Transistor Device. *ACS Sens.* **2016**, *1*, 295.